2016 IEEE International Conference on Robotics and Automation (ICRA)
Stockholm, Sweden, May 16-21, 2016

An Integrated Jumping-Crawling Robot using Height-Adjustable Jumping Module

Gwang-Pil Jung, Carlos S. Casarez, Sun-Pill Jung, Ronald S. Fearing and Kyu-Jin Cho, *Member, IEEE*

***Abstract*— In this paper, we propose a trajectory-adjustable integrated milli-scale jumping-crawling robot with improved ability to overcome obstacles compared to a robot that can only crawl. The robot employs a novel jumping module with enhanced energy storing-capacity and a height-adjustable active trigger. To increase the energy-storing capacity, latex rubber and knee-like joints are employed to utilize large displacement of the elastic material. The active trigger is based on a single DC motor and can release stored energy at any state, enabling the robot to control the take-off speed of jumping. The jumping module is integrated with the lightweight Dash crawler. The integrated jumping-crawling robot weighs 59.4 g and controls its moving trajectory by adjusting both its crawling speed and its jumping take-off speed.**

I. Introduction

Recent research on mobile milli-scale robots has focused on increasing their maneuverability by changing from single locomotion modes such as jumping, crawling, and climbing to forms of locomotion that integrate multiple movements (termed multi-modal locomotion). Milli-scale robots with multi-modal locomotion have been developed for two applications: reducing the cost of transport (CoT) and expanding locomotion domain.

Robots developed to reduce CoT combine jumping and gliding, "jump-gliding". [4-8]. Jump-gliding enables these robots to travel an extended horizontal distance for a given amount of stored energy. These robots can also achieve various trajectories and land on the ground gently.

Robots developed to expand locomotion domain often use an integrated crawling and jumping locomotion method [2, 9-12]. The same integrated crawling-jumping locomotion can easily be seen in small insects such as locusts, grasshoppers and froghoppers. During ordinary locomotion, these insects mainly use their four fore-legs to walk and crawl. But to escape from predators and to reach places where they cannot crawl, they use their relatively long and thick hind legs.

Inspired by such insects, milli-scale robots that use both crawling and jumping locomotions have been developed. Stoeter et al. [2] proposed a Scout robot that has two wheels for rolling and a winch for jumping into three-dimensional (3D) space. The robot can jump up to 30 cm by using its spring steel foot. While the Scout robot employs separate jumping and rolling motions, the Mini-Whegs™ robot developed by Lambrecht et al. [12] uses integrated running and jumping motions. The robot overcomes obstacles by jumping up to 18 cm (1.76 J/kg) while also crawling. These robots have successfully suggested the feasibility of expanding reachable domain by integrating crawling and jumping.

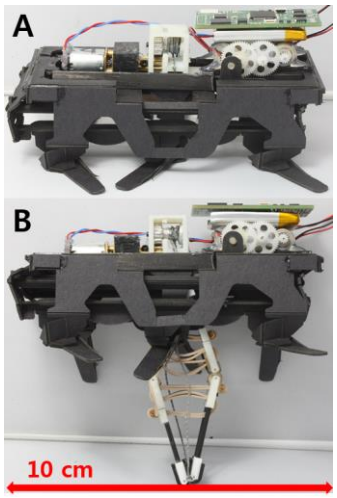

Fig. 1. The 59.4g integrated jumping-crawling robot in (a) the fully loaded stated and (b) the released stated.

In this paper, we propose a robot that can control its trajectory by adjusting both its crawling speed and its jumping take-off speed. The robot consists of a height-adjustable and powerful jumping mechanism that is integrated with the lightweight six-legged Dash crawler (Dash Robotics Inc.). The whole robot weighs 59.4 g and is shown in Fig. 1. Because the robot can jump from 1.10 m to 1.62 m and crawl at a speed of 0 m/s to 0.62 m/s, it can follow various trajectories of movement.

The paper is organized as follows: The design section describes the structure of the mechanism, material selection, and how we maximized the mechanism's energy-storing capacity. The modeling section considers both static and

TABLE I. Existing Jumping-Crawling Robots

Robots	Mass (g)	Size (cm)	Jumping height (m)	Jumping distance (m)
Scout [2]	200	11.5	0.57	-
MiniWheg [12]	191.4	10.4	0.18	-
Proposed robot	59.4	10.0	1.62	0.6

* This research was supported by a grant to Bio-Mimetic Robot Research Center, funded by Defense Acquisition Program Administration under the grant number UD130070ID.

G. P. Jung, S. P. Jung, and K. J. Cho are with the Biorobotics Laboratory, School of Mechanical & Aerospace Engineering/IAMD, Seoul National University, Seoul, Republic of Korea.

Carlos S. Casarez and Ronald S. Fearing are with the Department of Electrical Engineering and Computer Sciences, University of California, Berkeley, CA 94720, USA. (corresponding author: 82-2-880-1703, fax: 82-2-880-1663, kjcho@snu.ac.kr)

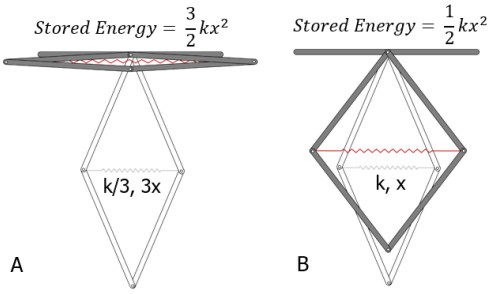

Fig. 2. Storable energy depends on the spring constant and displacement, assuming that both structures have the same force limit, $F = kx$.

dynamic modeling of the loading force and dynamic motion of the jumping mechanism. The experiments section describes the results of experiments to assess the robot's ability to overcome obstacles.

II. Jumping Module Design

The jumping module is developed to satisfy two design requirements. First, the jumping module needs to have an energy-storing capacity of more than 46.7 J/kg (1.4 J in 30.0 g module) to allow the whole system to jump to height of 2m, assuming that the mass of the whole system is about 60.0g.

The value of 46.7 J/kg is quite large amount in milli-scale jumping robots. To our knowledge, a 7 g jumping robot [14] has energy-storing capacity of about 21.9 J/kg, which is the largest amount of stored energy among current milli-scale robots.

To increase energy-storing capacity, our approach begins with the basics. Fig. 2 shows two structures that have a force limit of kx, where k is the spring constant and x is the displacement. The structure in Fig. 2 (a) stores the energy of $3kx^2/2$ while the structure in Fig. 2 (b) stores $kx^2/2$. This suggests that large displacement rather than large spring constant can increase energy-storing capacity. To implement this basic principle, we employ a hyperelastic material to utilize large strain of the material. We also employed a fully compressible linkage shown in Fig. 2 (a) and a knee-like joint to easily lengthen the material (shown in Fig. 6).

The second design requirement is that the jumping module should be able to actively release the stored energy, irrespective of the quantity of energy stored, to control the take-off speed of jumping. To this end, a novel active triggering mechanism based on a single DC motor is designed.

TABLE II. Material Propeties [1]

Materials	Young's Modulus (GPa)	Energy /Vol (mJ/mm^3)	Energy /Mass (J/kg)	Dissipation factor at 1kHz
Silicon	190	0.66	280	-
Resilin	0.002	2.25	2100	-
PDMS	0.00075	3.3	3400	-
Polyurethane	0.0076	95	76000	0.034
Latex	0.0001	5	4000	0.005

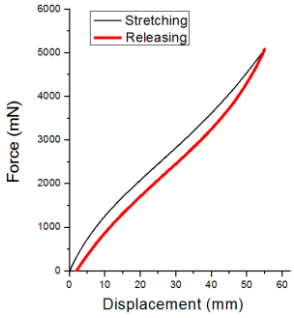

Fig. 3. Experimental results of stretching latex. The specimen is 5.5 mm wide, 25 mm long, and 0.85 mm thick.

A. Energy Storing Material

Spring steel has been widely employed for energy-storing components due to its easy accessibility. However, according to [15], spring steel is not a very efficient energy-storing material because of its high density. Instead of spring steel, we employ rubber material in the jumping module since it has an outstanding energy density compared to other materials [15]. However, rubber generally shows large hysteresis in its force-displacement curve. Table II shows the properties of five possible materials. Polyurethane has high energy density but also a high loss factor [1]. In contrast, latex has relatively low energy density and modulus but can be stretched by more than 250% and has small hysteresis in its force-displacement curve [1], as shown in Fig. 3. Latex therefore fit our design requirement to maximize energy-storing capacity.

B. Structure of the Jumping Module

The structure of the jumping module utilizes a simple diamond-shaped four-bar linkage to lengthen the latex as shown in Fig. 4. As the structure is compressed, the latex stretches and the amount of stored energy increases. Fig. 4 (a) shows the mechanism with a full load of stored energy, and

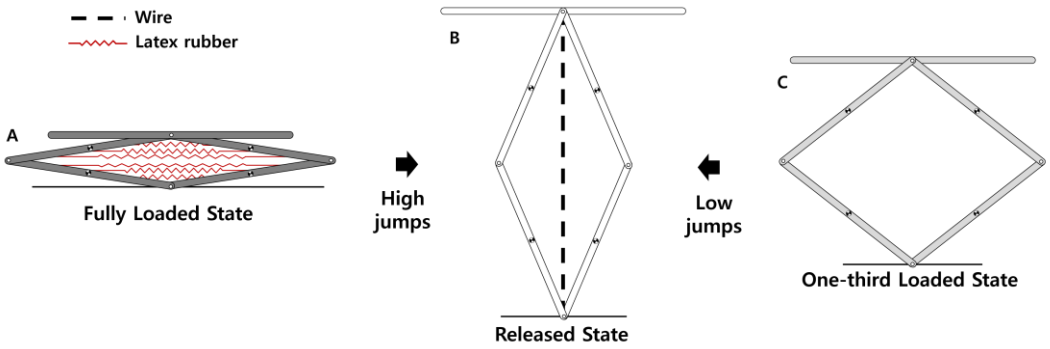

Fig. 4. Conceptual models of the proposed jumping mechanism in (a) the fully loaded state, (b) the released state, and (c) the one-third loaded state. The mechanism can jump from both the fully loaded state and the one-third loaded state depending on the required jumping heights

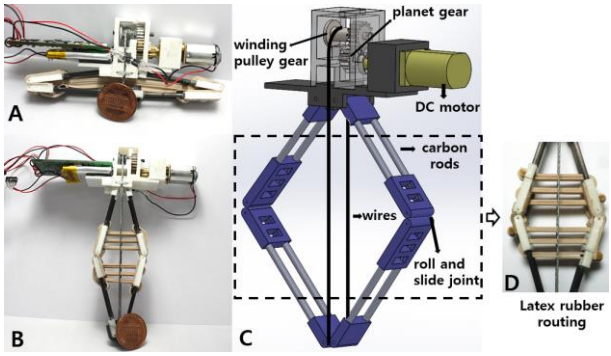

Fig. 5. (a) The jumping module in (a) the state of fully stored energy and (b) the released state. (c) 3D CAD model of the entire jumping module. (d) Latex rubber routing.

Fig. 4 (c) shows it at one-third of its full capacity. The stored energy is released by decompressing the structure, as shown in Fig. 4 (b).

Fig. 5 (c) shows the 3D CAD model of the entire jumping module. A pair of wires is attached at both sides, and a pulley winds the wires to compress the structure. When this occurs, the routed latex rubber stretches and stores energy, as shown in Fig. 5 (d).

C. *Roll and Slide Joints with Crossed Flexures*

The degree to which the jumping structure can be compressed basically depends on the range of motion of its joints. If the joints have little range of motion, then the structure cannot be fully compressed or decompressed. To solve this issue, we developed a rolling and sliding joint inspired by the human knee, as shown in Fig. 6 [16].

The joint shown in Fig. 6 (a) can be fully folded and unfolded, just like the human knee. The joint consists of three crossed flexures and a lateral wire. The lateral wire basically connects two linkages. The crossed flexure enables the joint to be robust to compressive force. A joint without a flexure tends to deviate from the center when compressive force is exerted as shown in Fig. 6 (c). The crossed flexure, however, prevents the joint from deviating, as can be seen in Fig. 6 (b).

D. *Height-Adjustable Triggering Mechanism*

The second design requirement is active release of stored energy to control take-off speed of jumping. The mechanism in Fig. 7 consists of a winding pulley gear, a planet gear and a motor gear. The planet gear rotates around the motor gear and contacts and detaches from the winding pulley gear depending on rotational direction of the motor gear. When the motor rotates clockwise, the planet gear contacts the winding pulley gear and starts to wind the wires. When the motor rotates counter-clockwise, the planet gear detaches from the winding pulley gear, and the winding pulley gear is released. With this active triggering mechanism, the jumping module can be released at any state, as shown in Fig. 4, which enables control of the take-off speed of jumping.

III. Integrated Jumping-Crawling Robot

The jumping module is integrated with a lightweight Dash crawler. The crawler has a vacant space inside its body of 100 mm length x 20 mm width x 35 mm depth. The jumping module is installed inside the crawler as shown in Fig. 8.

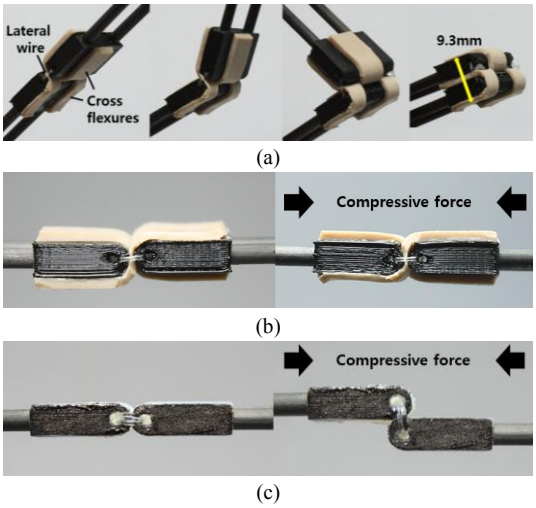

Fig. 6. Knee-inspired roll and slide joint. (a) From the flat state to the fully folded state. Joints in compressive force of 35N (b) with cross flexures and (c) without cross flexures.

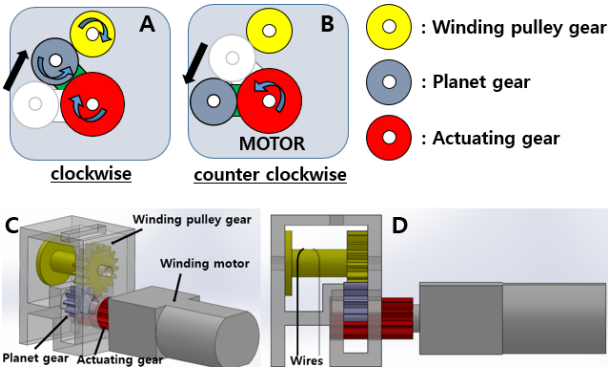

Fig. 7. (a), (b) Conceptual diagram of the active triggering mechanism using a single DC motor. (c), (d) Magnified 3D CAD view of the triggering mechanism.

The jump-crawler's stored elastic energy is adjusted according to the target take-off speed of jumping. When the robot needs to jump high, the motor fully winds the pulley wires to store more elastic energy, as shown in Fig. 8 (a). When the robot needs to make a low jump, the motor winds the wires less, and the jumping module is only partially compressed, as shown in Fig. 8 (b). When the module is compressed to less than 35 mm, the jumping structure does not touch the ground at all, and the robot can crawl as normal.

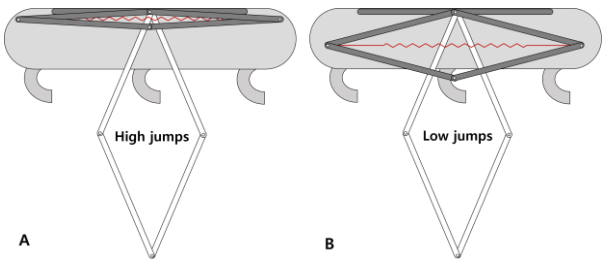

Fig. 8. Conceptual model of the height-adjustable integrated crawling-jumping robot, showing the state of the mechanism for (a) high jumps and (b) low jumps.

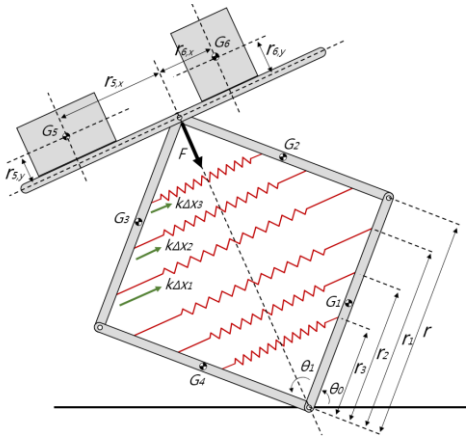

Fig. 9. Dynamic model of the proposed mechanism. G5 and G6 indicate the payload such as a battery, electronics, and an actuator.

The diamond structure of the jumping module is located at the center of the robot, which distributes the mass distribution to reduce rotational motion when the robot jumps. The mass budget of whole system is given in Table III.

The robot is controlled by the dsPIC33JF128MC706-based board [17]. The board uses an 802.15.4 wireless radio and two H-bridge motor controller. The crawler uses two 7 mm-diameter, 3.3 Ω brushed DC motors (Didel MK07-3.3) and is controlled by changing the PWM ratio. The jumping module uses a DC motor (Pololu 1000:1 gear ratio) and a simple direction control is applied to store and release the energy.

IV. MODELING

To investigate how much force is required to load the proposed jumping mechanism, we created a static model. Using this model, the required loading force according to the shape of the jumping module is calculated.

Also, the jumping dynamics is analyzed based on the Lagrangian formulation. The process of jumping is completed within only 30 ms. Therefore, dynamics should be considered to precisely examine how the mechanism works. Based on the dynamic model, the take-off time, velocity, and energy used for jumping can be calculated.

TABLE III. MASS BUDGET

Components	Mass (g)
Jumper transmission	4.8
Carbon rods (8 ea)	2.0
Joints (8 ea)	4.0
Wire, joint rubber	2.2
Jumper motor	11.0
Latex rubber for energy storage (2 ea)	2.2
Control board	6.9
Li-Po Battery	5.3
Crawler body	16.0
Crawler transmission	5.0
Total	59.4

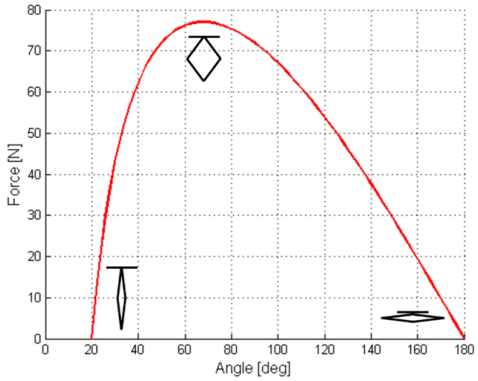

Fig. 10. Loading force vs. angle.

A. Loading Force Analysis

To select the actuator to load the mechanism, a static loading force analysis is performed. Fig. 9 shows the model of the proposed mechanism. The model represents the routed latex rubber as six symmetrically positioned springs in the upper triangle and the lower triangle, as shown in Fig. 9. The three springs in each triangle have the spring constant of k_1, k_2 and k_3, which are determined by tensile tests. The loading force, F, can be calculated based on the moment equilibrium equation as follows:

$$rFsin\theta' = r_1k_1\Delta x_1cos\theta' + r_2k_2\Delta x_2cos\theta' + r_3k_3\Delta x_3cos\theta' \quad (1)$$

where $\Delta x_i = r_i(sin\theta' - sin\theta'_{initial})$, $\theta' = \theta_1/2$ and $\theta'_{initial} = \theta_{1,initial}/2$

$$F = \frac{8(r_1{}^2k_1+r_2{}^2k_2+r_3{}^2k_3)(sin\theta'-sin\theta'_{initial})cos\theta'}{rsin\theta'} \quad (2)$$

where $r_1 = 41mm$, $r_2 = 36mm$, $r_3 = 31mm$, $r = 45mm$, $k_1 = 172.86N/m$, $k_2 = 200.14N/m$, $k_3 = 216.5N/m$ and $\theta'_{initial} = 20^\circ$.

Based on eq. (2), the relation between the loading force and the angle, θ_1, is given in Fig. 10. In this figure, the peak loading force is 77.0 N. Given that the stall torque of the DC motor is 0.9 Nm, the radius of the pulley should not exceed 11.6 mm as follows:

$$Pulley\_radius_{max} = \tau/F_{peak} = 0.900\text{Nm}/77.0\text{N} = 11.6 \text{ mm} \quad (3)$$

The pulley used in the mechanism has a radius of 2 mm and produces enough force for loading.

B. Dynamics

The model consists of five rigid links and four rotational joint. To analyze the dynamics, two variables (θ_1 and θ_0) are used to indicate the position of each link. The model is a one-degree-of-freedom system and has a generalized coordinate of the body angle, θ_1. The position of the links is given as follows:

$$\vec{G}_1 = \begin{bmatrix} \frac{1}{2}r\cos\theta_0 \\ \frac{1}{2}r\cos\theta_0 \end{bmatrix} \quad (4)$$

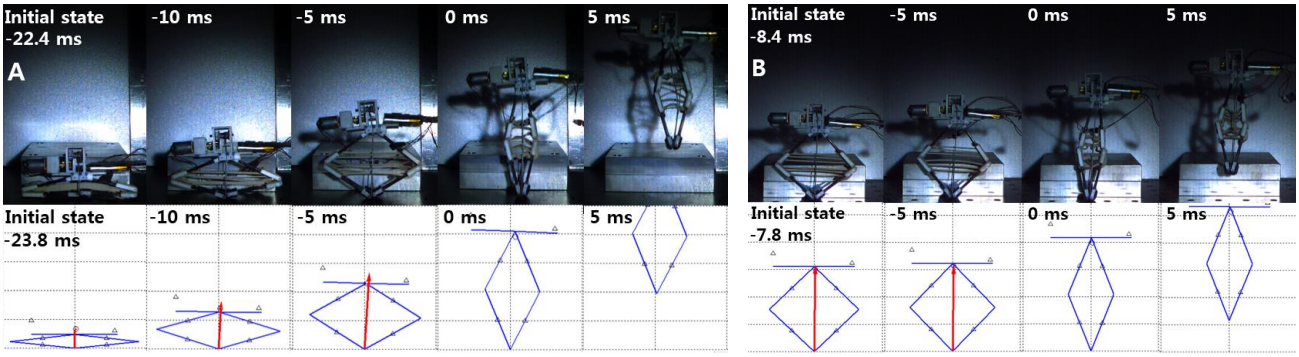

Fig. 11. High-speed (5000 fps) image of the jumping module and visualizatin of dynamic modeling of its movements. The red arrow indicates the direction of reaction force from the ground.

$$\vec{G}_2 = \begin{bmatrix} r\cos\theta_0 + \frac{1}{2}r\cos(\theta_0+\theta_1) \\ r\sin\theta_0 + \frac{1}{2}r\sin(\theta_0+\theta_1) \end{bmatrix} \quad (5)$$

$$\vec{G}_3 = \begin{bmatrix} r\cos(\theta_0+\theta_1) + \frac{1}{2}r\cos\theta_0 \\ r\sin(\theta_0+\theta_1) + \frac{1}{2}r\cos\theta_0 \end{bmatrix} \quad (6)$$

$$\vec{G}_4 = \begin{bmatrix} \frac{1}{2}r\cos(\theta_0+\theta_1) \\ \frac{1}{2}r\sin(\theta_0+\theta_1) \end{bmatrix} \quad (7)$$

$$\vec{G}_5 = \begin{bmatrix} r\cos\theta_0 + \frac{1}{2}r\cos(\theta_0+\theta_1) - \\ \qquad r_{5,y}\cos\left(\theta_0+\frac{1}{2}\theta_1\right) - r_{5,x}\sin(\theta_0+\frac{1}{2}\theta_1) \\ r\sin\theta_0 + \frac{1}{2}r\sin(\theta_0+\theta_1) + \\ \qquad r_{5,y}\sin\left(\theta_0+\frac{1}{2}\theta_1\right) + r_{5,x}\cos(\theta_0+\frac{1}{2}\theta_1) \end{bmatrix} \quad (8)$$

$$\vec{G}_6 = \begin{bmatrix} r\cos\theta_0 + \frac{1}{2}r\cos(\theta_0+\theta_1) - \\ \qquad r_{6,y}\cos\left(\theta_0+\frac{1}{2}\theta_1\right) + r_{6,x}\sin(\theta_0+\frac{1}{2}\theta_1) \\ r\sin\theta_0 + \frac{1}{2}r\sin(\theta_0+\theta_1) + \\ \qquad r_{6,y}\sin\left(\theta_0+\frac{1}{2}\theta_1\right) - r_{6,x}\cos(\theta_0+\frac{1}{2}\theta_1) \end{bmatrix} \quad (9)$$

where G_i is the position of links, r is the length of each link of the diamond-shaped body, $r_{5,x}$, $r_{5,y}$, $r_{6,x}$, and $r_{6,y}$ are the distance to added masses.

θ_1 is the angle of the diamond. θ_1 and θ_0 have the following relationship:

$$\theta_0 = (180° - \theta_1)/2 \quad (10)$$

With the positions and the kinematic constraints, the dynamics of the jumping module are numerically solved by a Lagrange formulation. The initial conditions are set as follows:

$$\theta_1 = 170° \text{ at fully stored state} \quad (11)$$

TABLE IV. COMPARISON OF EXPERIMENT AND MODELING

-	High jumps		Low jumps	
	Model	Exp.	Model	Exp.
Take-off time (ms)	23.8	22.4	7.80	8.40
Take-off speed (m/s)	7.81	7.71	4.57	4.49
Initially stored energy (J)	1.39	1.39	0.49	0.49
Actual used energy (J)	1.16	1.1	0.40	0.39
Conversion efficiency (%)*	83	79	82	79
Jumping height (m)	-	2.90	-	1.10

*Conversion efficiency is the ratio of initially stored energy to actual kinetic energy at take-off [3], [13].

Take-off of the jumping mechanism occur when the vertical reaction force, $V(t)$ in (13), is zero.

$$m_{robot}a_{robot,x} = \sum_{i=1}^{6} m_i a_{i,x}(t) = -H(t) \quad (12)$$

$$m_{robot}a_{robot,y} = \sum_{i=1}^{6} m_i a_{i,y}(t) = V(t) - \sum_{i=1}^{6} m_i g \quad (13)$$

where m_{robot} is the total mass of the robot, a_{robot} is the acceleration of the robot's center of mass, a_i is the acceleration of each link, and H is the horizontal reaction force on the ground. Also, the take-off translational velocity, (14), and the angular velocity, (15), are determined as follows:

$$m_{robot}v_{robot} = \sum_{i=1}^{6} m_i v_{i,f} \quad (14)$$

$$m_{robot}w_{robot} = \sum_{i=1}^{6} m_i w_{i,f} \quad (15)$$

where v_{robot} is the velocity of the robot's center of mass and w_{robot} is the angular velocity of the robot. $v_{i,f}$ is the translational velocity, and $w_{i,f}$ is the angular velocity of each link just before takeoff.

V. EXPERIMENTAL RESULTS

The jumping module is designed to satisfy two design requirements: Large energy-storing capacity and height-adjustable triggering. To examine the functionality of the jumping module, we test jumping by varying the quantity of stored energy in the jumping module and integrated jumping-crawling by adjusting different take-off and crawling speeds.

To operate the robot, a LiPo battery (3.7V, 370mAh) is used. The jumping mechanism requires 240mA for 28s to fully charge the jumping energy and the crawler consumes about 600mA continuously.

A. Jumping Experiment

The jumping experiments are done by varying the quantity of stored energy. Fig. 11 shows high-speed images and corresponding dynamic models of jumping at two different initial states. In Fig. 11 (a) the module initially has 1.39 J of elastic energy, and in Fig. 11 (b) it has 0.49 J.

In Fig. 11 (a), the jumping module takes off within 22.4 ms with a speed of 7.71 m/s and jumps to 2.90 m. The module actually uses 1.1 J, which is 79% of its initially stored energy. The jumping module in Fig. 11 (b) initially stores 0.49 J and uses 0.39 J which is 79% of its initially stored energy. The module takes off within 8.40 ms with a speed of 4.49 m/s and jumps up to 1.10 m.

Table 2 compares data from the experiment and the model. Both sets of data shows similar values but have slight differences in the conversion efficiency, which is the ratio of

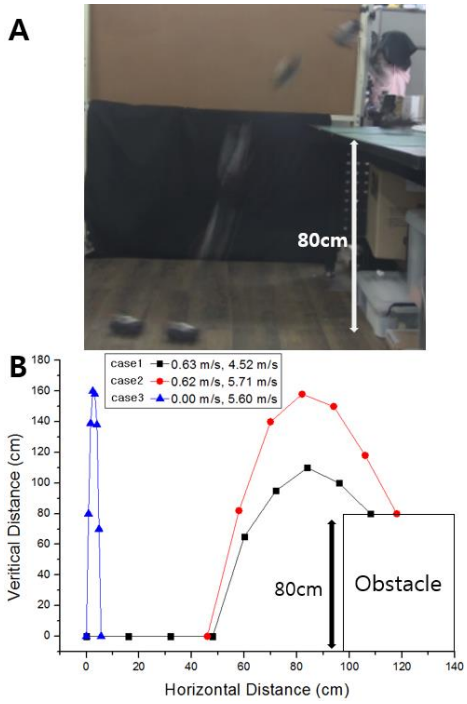

Fig 12. (a) Integrated jumping-crawling to overcome an 80-cm obstacle. (b)Vertical and horizontal distance of the integrated jumping-crawling robot. Numbers in the figure key are crawling speed and take-off speed. The time between dots is 0.168s.

the initially stored energy to the actual used energy. This error may come from a small degree of hysteresis in the latex rubber since the latex is modeled as a perfect linear spring for simplicity.

B. Integrated Jumping-Crawling Experiments

The integrated jumping-crawling robot is tested by varying crawling speed and take-off speed. Fig. 12 (a) shows the robot with crawling speed of 0.63 m/s and take-off speed of 4.52 m/s. This combined motion enables the robot to jump 1.10 m and overcome 0.80 m high obstacle.

Fig. 12 (b) shows the horizontal and vertical distances achieved in three different cases. In case 3, when the robot has a crawling speed of 0 m/s and a take-off speed of 5.60 m/s, it jumps nearly vertically. In case 1 and 2, the robot moves with almost equal crawling speed but different take-off speeds. In case 1 the robot's jumping module has 0.98 J of initially stored energy and jumps to 1.10 m. In case 2, the fully loaded jumping module has 1.39 J of stored energy, and jumps to 1.62 m. In the horizontal direction, in cases 1 and 2 the robot crawled 0.48 m and 0.60 m, respectively. The robot has an average horizontal moving speed in cases 1 and 2 of 0.57 m/s and 0.59 m/s, respectively, which means that crawling speed and take-off speed are independently controlled.

VI. CONCLUSION

In this paper, we propose a trajectory-controlled integrated jumping-crawling robot. To this end, a novel jumping module is developed with a large energy-storing capacity and a height-adjustable active trigger. To increase the energy-storing capacity, the jumping module incorporates latex rubber and knee-like joints. These components enables the jumping module to utilize large displacement of material, which is our strategy for maximizing energy-storing capacity. Also, a novel active trigger is designed to release the stored energy at any state. The trigger uses only a single DC motor and works by controlling the direction of rotation. With this trigger, the jumping module can control its jumping height. The developed jumping module is integrated with a lightweight Dash crawler. The whole system weighs 59.4 g and achieves different trajectories by controlling crawling speed and take-off speed.

REFERENCES

[1] S. E. Bergbreiter, "Autonomous Jumping Microrobots," 2007.

[2] S. A. Stoeter and N. Papanikolopoulos, "Kinematic Motion model for jumping scout robots," 2006.

[3] J. Burdick and P. Fiorini, "Minimalist jumping robots for celestial exploration," *The International Journal of Robotics Research,* vol. 22, pp. 653-674, 2003.

[4] M. A. Woodward and M. Sitti, "MultiMo-Bat: A biologically inspired integrated jumping-gliding robot," *The International Journal of Robotics Research,* vol. 33, pp. 1511-1529, 2014.

[5] A. Vidyasagar, J. C. Zufferey, D. Floreano, and M. Kovac, "Performance analysis of jump-gliding locomotion for miniature robotics," *Bioinspir Biomim,* vol. 10, p. 025006, 2015.

[6] A. L. Desbiens, M. T. Pope, D. L. Christensen, E. W. Hawkes, and M. R. Cutkosky, "Design principles for efficient, repeated jumpgliding," *Bioinspir Biomim,* vol. 9, p. 025009, Jun 2014.

[7] M. Kovac, "EPFL jumpglider: A hybrid jumping and gliding robot with rigid or folding wings," *2011 IEEE/RSJ International Conference on Robotics and Biomimetics,* 2011.

[8] M. A. Woodward and M. Sitti, "Design of a Miniature Integrated Multi-Modal Jumping and Gliding Robot," *2011 IEEE/RSJ International Conference on Intelligent Robots and Systems,* pp. 556-561, 2011.

[9] J. Zhao, J. Xu, B. Gao, N. Xi, F. J. Cintr´on, M. W. Mutka, and L. Xiao, "MSU Jumper: A Single-Motor-Actuated Miniature Steerable Jumping Robot," *Robotics, IEEE Transactions on,* vol. 29, pp. 602-614, 2013.

[10] R. Armour, K. Paskins, A. Bowyer, J. Vincent, and W. Megill, "Jumping robots: a biomimetic solution to locomotion across rough terrain," *Bioinspiration & Biomimetics,* vol. 2, pp. S65-S82, 2007-09-01 2007.

[11] H. Tsukagoshi, M. Sasaki, A. Kitagawa, and T. Tanaka, "Design of a higher jumping rescue robot with the optimized pneumatic drive," in *Proceedings of the IEEE International Conference on Robotics and Automation (ICRA)*, 2005, pp. 1276-1283.

[12] B. G. A. Lambrecht, A. D. Horchler, and R. D. Quinn, "A Small, Insect-Inspired Robot that Runs and Jumps," in *Proceedings of the IEEE International Conference on Robotics and Automation*, 2005, pp. 1240 - 1245.

[13] G. P. Jung, J. S. Kim, J. S. Koh, S. P. Jung, and K. J. Cho, "Role of compliant leg in the flea-inspired jumping mechanism," in *IEEE/RSJ International Conference on Intelligent Robots and Systems (IROS)*, 2014, pp. 315-320.

[14] M. Kovac, M. Fuchs, A. Guignard, J. C. Zufferey, and D. Floreano, "A miniature 7g jumping robot," in *IEEE International Conference on Robotics and Automation (ICRA)*, 2008, pp. 373 -378.

[15] M. F. Ashby and D. Cebon, "Materials selection in mechanical design," *Le Journal de Physique IV,* vol. 3, pp. C7-1-C7-9, 1993.

[16] E. Pena, B. Calvo, M. Martinez, and M. Doblare, "A three-dimensional finite element analysis of the combined behavior of ligaments and menisci in the healthy human knee joint," *Journal of Biomechanics,* vol. 39, pp. 1686-1701, 2006.

[17] S. S. Baek, F. L. Garcia Bermudez, and R. S. Fearing, "Flight control for target seeking by 13 gram ornithopter," in *Intelligent Robots and Systems (IROS), 2011 IEEE/RSJ International Conference on*, 2011, pp. 2674-2681.